Transitions and Pressure Drop Characteristics of Flow in Channels with Periodically Grooved Parts.

Takahiro ADACHI[*1] and Haruo UEHARA[*2]

[*1] OTEC Laboratory, Saga University, Honjo, Saga 840-8502, Japan
[*2] Department of Mechanical Engineering, Saga University, Honjo, Saga 840-8502, Japan

Abstract

Transitions of flow in periodically grooved channels and pressure drop characteristics are numerically investigated by assuming two-dimensional and fully developed flow fields. It is confirmed that a self-sustained oscillatory flow occurs at a critical Reynolds number from the steady state flow as a Hopf bifurcation due to the instability. The critical Reynolds numbers are obtained for various channel geometries. The ratio of the pressure drop to that of parallel plate channel is also investigated. It is shown that the ratio is less than unity for the expanded channel geometries for the subcritical Reynolds numbers.

NOMENCLATURE

A : amplitude parameter
a_u : upper height of contracted or expanded part from the centerline
a_l : lower height of contracted or expanded part from the centerline
h : half height of the parallel plane channel
L : period of the module
l : length of contracted or expanded part
p : pressure
Re : Reynolds number, $Re = U^* h^* / \nu^*$
T : period of oscillation
U_m^* : mean velocity
U^* : representative velocity, $U^* = \frac{3}{2} U_m^*$
u, v : velocity components in $x-$ and $y-$ directions, respectively
$\mathbf{u}$: velocity vector

Greek symbols
Δp : pressure drop
Δt : time increment
Δx, Δy : grid size, $\Delta x = \Delta y$ in this study
ϵ : relaxation factor
λ : coefficient of the pressure drop
ν^* : kinematic viscosity
ρ^* : density
σ : growth rate
ψ : nondimensional stream function
Ω : frequency, $\Omega = 1/T$
ω : nondimensional vorticity

Subscripts
c : critical
p : plane Poiseuille flow
$*$: dimensional value

1 INTRODUCTION

Flow over grooves and in grooved channel often arises in plate-type heat exchanger devices which are extensively used in many applications as a compact and less expensive heat exchanger. The spatially periodic grooves are often set up between the parallel plates of the plate-type heat exchanger in order to enhance the heat transfer rate, because the grooves induce the flow separation and interrupt the development of the thermal boundary layer[1]. It has been shown that heat transfer rate is enhanced by the factor of three or four times larger than that for simple parallel plate channel by setting up grooves, but it leads to serious increase of the pressure drop at the same time. Thus, it is expected to extend the knowledge of an effect of grooves on pressure drop characteristics as well as heat transfer enhancements

Several numerical studies of fully developed flow in channels with periodically varying cross-section have been presented in the past, where the channels are divided into identical modules in the streamwise direction where the fully developed velocity field repeats itself in a cyclic manner[2]-[4]. The influence of the entrance region can be neglected if the channel are long and many modules are presented. This enables us to divide the channels into identical modules and to confine the calculation domain to cover only one of these modules without dealing with the entrance region. Such a procedure was first suggested by Patankar et al.[2] and was applied to a configuration consisting of successive ranks of isothermal plate segments placed transverse to the main flow direction under steady state conditions. These assumptions are supported by experimental investigations by several authors[5]-[8],

In this paper, we investigate the flow in channels with rectangular grooves as a simple model of the plate-type heat exchanger. Sunden and Trollheden[9] studied the laminar

convective flow and heat transfer in channels with rectangular grooves on one plate under steady state conditions. Ghadder et al.[10] and Pereira and Sousa[11] calculated the time-dependent equation about the flow in the similar configuration with Sunden and Trollheden[9] and found that the steady state flow becomes periodic in time, that is to say, a self-sustained oscillatory flow at a critical value of the Reynolds number. A wave is generated for the self-sustained flow and this wave is identified as a T-S(Tollmien-Schlichting) wave. In addition to this, Ghadder et.al[10] showed that the pressure drop is less than the corresponding quantity for plane Poiseuille flow for the steady laminar flow, whereas increases for the self-sustained oscillatory one.

Roberts[12] studied the flow in a symmetric channel with baffles on both plates by numerical simulation and experiment with flow visualization. He showed that a steady symmetric flow at low Reynolds numbers becomes unstable as the Reynolds number increases, and the resultant flow is asymmetric and periodic in time. It was shown that a wave is generated by Kelvin-Helmholtz shear-layer instability.

The objective in this study is to reveal how transitions from steady state flow to self-sustained oscillatory one and the pressure drop characteristics of the flow are altered depending upon the effects of the channel geometries by using numerical simulation. So, we examine some channel geometries with contracted and expanded grooves set up both symmetrically and asymmetrically with the centerline of the parallel plates.

2 GOVERNING EQUATION

We consider a two-dimensional channel as shown in Fig. 1. The channel consists of parallel plates of height $2h^*$ with periodically contracted or expanded parts. Figure 1(d) is an enlargement of part A shown in Fig. 1(a), which is one of the periodic modules with periodicity length L^*. Fluid enters from an inlet far upstream and flows through the

entrance region, and arrives at the module.

The x-axis is taken in the flow direction and the y-axis is perpendicular to it with the origin O in Fig. 1(d). The flow is assumed to be two-dimensional and incompressible. The no-slip condition is used on the plates. We make all the physical quantities nondimensional by taking the half height of the plates h^* as a representative length and $U^* = \frac{3}{2}U_m^*$ (U_m^* is mean velocity at the cross-section of height $2h^*$) as a representative velocity, where we represent physical quantities with their dimension by attaching a superscript * with them. The governing equations for the vorticity $\omega(x, y, t)$ and the stream function $\psi(x, y, t)$ are written in nondimensional forms as

$$\frac{\partial \omega}{\partial t} + \frac{\partial \omega}{\partial x}\frac{\partial \psi}{\partial y} - \frac{\partial \omega}{\partial y}\frac{\partial \psi}{\partial x} = \frac{1}{Re}\left(\frac{\partial^2 \omega}{\partial x^2} + \frac{\partial^2 \omega}{\partial y^2}\right), \tag{1}$$

$$\omega = -\left(\frac{\partial^2 \psi}{\partial x^2} + \frac{\partial^2 \psi}{\partial y^2}\right). \tag{2}$$

The Reynolds number is defined as $Re = U^* h^*/\nu^*$. Moreover, as parameters to determine the configuration of the channel, period L of the channel, length l of the contracted or expanded grooves, and heights a_u, a_l of the grooves from the centerline of the parallel plates are defined as

$$L = L^*/h^*, \quad l = l^*/h^*, \quad a_u = a_u^*/h^*, \quad a_l = a_l^*/h^*, \tag{3}$$

where the channel consists of parallel plates without grooves for $a_u = a_l = 1$, whereas it has expanded parts if $a_u, a_l > 1$ and contracted parts if $a_u, a_l < 1$.

A pressure field is obtained by solving the Navier-Stokes equation as

$$\nabla p = -\frac{\partial \mathbf{u}}{\partial t} - (\mathbf{u} \cdot \nabla)\mathbf{u} + \frac{1}{Re}\nabla^2 \mathbf{u}, \tag{4}$$

where the velocity $\mathbf{u} = (u, v)$ is expressed in terms of the stream function ψ as $u = \partial\psi/\partial y$ and $v = -\partial\psi/\partial x$.

The boundary conditions on the plates are given as

$$\psi = 0, \quad u = \frac{\partial \psi}{\partial y} = 0, \quad v = -\frac{\partial \psi}{\partial x} = 0, \quad \text{on the lower plate,} \tag{5}$$

$$\psi = \frac{4}{3}, \quad u = \frac{\partial \psi}{\partial y} = 0, \quad v = -\frac{\partial \psi}{\partial x} = 0, \quad \text{on the upper plate,} \tag{6}$$

where the values of the stream function on the plates are determined from the flow rate in the cross section of the cancel which is constant being 4/3.

The flow is expected to attain, after a short entrance region, a periodic fully developed regime, in which the velocity field repeats itself from module to module. This expectation is validated by the results of Farhanieh et al.[5] and Roberts[12]. So, the following periodic boundary conditions are imposed at the inlet and outlet of the module

$$\psi(x + L, y, t) = \psi(x, y, t), \quad \omega(x + L, y, t) = \omega(x, y, t). \tag{7}$$

The boundary condition for the pressure p is given as $p = 0$ at the centerline of the inlet of the periodic module.

3 NUMERICAL METHOD

We solve the governing equations numerically by the time marching method. The vorticity transport equation (1) is approximated by the explicit Adams-Bashforth method with the second order accuracy in time together with the second order accuracy of central finite difference in space. The Poisson equation (2) is approximated by the second order central difference and solved by the SOR (Successive Over Relaxation) method, where the relaxation factor ϵ is constant and $\epsilon = 1.5$ is used. The convergence of the SOR method is determined when the maximum relative difference for the stream function reaches 10^{-5} in all grid points.

As a representative quantity for the flow field obtained by the numerical simulation, we adopt a y-component velocity v at $(x, y) = (L/2 + l/2, -0.5)$. The steady flow state is determined when the velocity v becomes independent of time and the maximum relative difference between successive time steps reaches 10^{-7}, otherwise it is judged as time dependent. In the case that the flow is time periodic oscillatory state, the calculation is terminated when the maximum relative difference for a local maximum amplitude of v between successive oscillation cycles reaches 10^{-4}.

Accuracy tests were performed for the channel geometry of $L = 8, l = 4, a_u = 1, a_l = 2$ and $Re = 400$. In our calculations, equally spaced mesh system is used. To study the effect of time increment Δt and grid sizes Δx and Δy on the solution, the following two systems are examined, that is, (i)$\Delta t = 0.001, \Delta x = \Delta y = 0.05$ and (ii) $\Delta t = 0.0001, \Delta x = \Delta y = 0.04$. Then, v at $(x, y) = (L/2+l/2, -0.5)$ converges on constant value of $v = 0.0123$ for the system of (i) and on $v = 0.0121$ for the system of (ii). It is confirmed that the relative error for v is within 2% with the difference of the two grid systems, and the time increment and grid sizes are small enough for the accuracy required. We use hereafter the grid system of (i) for $Re \leq 500$ and the system of (ii) $Re > 500$.

4 RESULTS

4.1 Flow Fields and Transitions

Numerical simulations are carried out for $L = 8$, $l = 4$, $a_l = 2$ which are fixed, and for five different values of $a_u = 0, 0.5, 1, 2$ and 3.

4.1.1 Steady flows

The streamlines of the steady state flow for $a_u = 1$ and $Re = 50$ and 380 are depicted in Fig. 2. In this case, the upper plate is flat and the lower has the expanded part, so the

channel is asymmetric. The flow is periodically fully developed and has the same period L as the module. A small circulation region can be seen at the upstream of the expanded part in Fig. 2(a) because the flow is not able to turn sufficiently sharp and can not follow the wall. The main flow is deflected into the expanded part. The circulation grows larger and its center moves to the downstream as the Reynolds number increases and occupies whole region of the expanded part for $Re = 380$. The main flow for $Re = 380$ becomes straight without deflecting and the streamlines come to parallel as well as the profile of a plane Poiseuille flow, so a shear layer between the main flow and the flow inside the expanded part is established. There are some previous studies for the similar geometry with $a_u = 1$, and our pictures shown here are qualitatively the same as them[9]-[11]

Next, the streamlines of the steady flow for $a_u = 2$ and $Re = 50$ and 260 are shown in Fig. 3. In this case, the channel is symmetric with the centerline of parallel plates. Mizushima et al.[13] studied the stability of flow in a channel with single sudden expanded part and showed that the steady flow becomes asymmetric and deflects into one side of the expanded parts by a symmetry-breaking pitchfork bifurcation as the Reynolds number increases when $l/(a_u + a_l) > 2.3$. In our study, however, $l/(a_u + a_l) = 2$ and the flow is symmetric with the centerline of the channel without deflecting into one side. There are also small circulation regions for $Re = 50$ and they grow larger as the Reynolds number increases. They occupy whole region of the expanded part for $Re = 260$ and the centers move to the downstream of the expanded parts. The shear layer between the main flow and the flow inside the expanded part is also established here.

Finally, the streamlines of the steady flow for $a_u = 0$ and $Re = 50$ and 100 are depicted in Fig. 4. In this case, the upper plate has a contracted part and the lower has an expanded part, so the channel is asymmetric. It is seen that the streamlines meander along the channel geometry in Fig. 4(a) and the main flow goes deep in the grooves

(expanded part and groove formed by the contracted part). Small circulation regions for $Re = 50$ also grow larger as the Reynolds number increases and occupy whole region of the grooves for $Re = 100$ establishing the shear layer, and the centers move to the downstream of the grooves. It is seen that the main flow is restricted the half region of the original parallel plate with height $2h^*$ because the upper plate is contracted.

4.1.2 Oscillatory flows

In general, as the Reynolds number further increases, the steady state flow becomes unstable for infinitesimal disturbances and bifurcates to a time-periodic, self-sustained oscillatory flow at a critical Reynolds number Re_c.

Time evolutions of v at $(x, y) = (L/2 + l/2, -0.5)$ for $a_u = 2$ are shown in Fig. 5 for $Re = 250$ and 350 as an example of the transition. The behavior of the velocity v as a function of time at $Re = 250$ indicates a constantly decaying amplitude and converges to constant becoming invariant with time in Fig. 5(a). On the other hand, at a higher Reynolds number, $Re = 350$, the velocity has converged asymptotically to a periodic state with fixed oscillatory amplitude after a long elapse as shown in Fig. 5(b). This implies that the critical Reynolds number for onset of the self-sustained oscillatory flow is somewhere between 250 and 350.

To determine the dependence of the oscillation amplitude on degree of criticality, we define a pointwise amplitude parameter $A = |v - \bar{v}|^2_{max}$, where the overbar denotes time-average. The critical Reynolds number is obtained as the point where A changes from $A = 0$ to $A \neq 0$. In Fig. 6, we plot this amplitude parameter for each a_u as a function of Re. The curve of A in Fig. 6 suggests a linear dependence, $A \sim (Re - Re_c)$ near the critical point. This leads us to the conclusion that the transition from the steady flow to the time-periodic self-sustained oscillatory flow is caused by a regular Hopf bifurcation[14].

We have done a least-square fit for some points near the critical point, and plotted the results of this fit by dot-dashed lines in Fig. 6, where it is seen that, as expected, the agreement is quite good. Thus we can conclude that the self-sustained oscillations for each a_u occur as a result of the Hopf bifurcation.

The critical Reynolds numbers and the frequencies for each a_u are tabulated in Table. 1. The following equations for Re_c are obtained by just fitting the numerical data for $a_u \geq 1$ and $a_u \leq 1$, assuming an asymptotic value $Re_c \to 0$ as $a_u \to -1$ because the channel is closed for $a_u = -1$,

$$Re_c = 187{a_u}^{-1.43} + 222 \quad \text{for } 1 \leq a_u \leq 3, \tag{8}$$

$$Re_c = 123(a_u + 1)^{1.74} \quad \text{for } 0 \leq a_u \leq 1. \tag{9}$$

These equations are reliable within 4% of relative error for the numerical data as shown in Fig. 7.

It has been found that the self-sustained oscillatory flow occurs as a result of the Hopf bifurcation. On the basis of these observations, we will next consider a disturbance which induces the Hopf bifurcation. Ghadder et al.[10] and Pereira et al.[11] showed that the disturbance for the similar geometry with $a_u = 1$ is a T-S(Tollmien-Schlichting) wave mode which destabilizes the Poiseuille flow in parallel plate channel, and the proposed mechanism of the generation of the T-S mode is the Kelvin-Helmholtz shear layer instability at the groove lip. Especially, Ghadder et al.[10] obtained the dispersion relation between a wave number $\alpha = 2\pi n/L$ and a frequency Ω for the effect of some values of L and l, where n is the number of waves that spans the periodicity length L, and showed that Ω for grooved channels agree almost exactly with the T-S mode for parallel plate channel. In the present study, it is shown that $\Omega = 0.115$ for $a_u = 1$ at the critical Reynolds number also practically agree with the T-S mode, $\Omega_{TS} = 0.121$, where $\Omega = 1/T$ is determined as a reciprocal of period T given by a typical crest-to-crest or through-to-through distance

from the time-history plots.

On the other hand, Roberts[12] studied the flow in a symmetric channel with periodically placed sharp edged baffles which corresponds to the similar geometry with $a_u = 2$ in this study but the thickness of the baffles are neglected as $l/L \to 1$. He showed that the instability mode which induces the Hopf bifurcation is the Kelvin-Helmholtz shear layer instability mode instead of the T-S mode. However, there is a thickness of baffle in our study and $l/L = 0.5$. It is unclear that the instability mode in the present study depends on which modes, because it is expected that the instability mode approaches the T-S mode for the opposite limit as $l/L \to 0$, that is, channel without grooves. And the instability modes of the other geometries for each a_u are also unclear. So, we henceforth focus our attention on the disturbances for $a_u = 0$ and 2 as typical cases.

We show instantaneous streamlines of self-sustained oscillatory flow at every one sixth period arbitrary from time $t = t_0$ for $a_u = 0$ and 2 in Figs. 8 and 9, where the Reynolds numbers are slightly larger than the critical values. The recirculation eddies in the grooves repeat a process that they are promoted to the downstream so as to be pressed against the wall of grooves, and moreover secondary vortices are born in the upstream. It is seen that a difference of a phase for the upper and lower circulation regions is half period in time and the same phenomena occur for every half period alternately in the upper and lower grooves. It is emphasized that there is significant waviness at the groove lip as compared with the steady case shown in Figs. 3 and 4, which is suggestive of similar patterns observed in Kelvin-Helmholtz instability of free shear layers.

The mean flow fields averaged in one period with time are shown in Figs. 10 and 11 for $a_u = 0$ and 2. Furthermore, the difference between the mean flow and the instantaneous streamline of self-sustained oscillatory flow which is called a disturbance in the nonlinear stability theory are shown in Figs. 12 and 13 at every one sixth period for $a_u = 0$ and

2. Thus, the disturbance profile is calculated by subtracting the mean flow field from the self-sustained flow field. The mean flow fields have similar flow patterns to those of the steady state just before the bifurcation depicted in Figs. 3(b) and 4(b). This implies that the disturbances shown in Figs. 12 and 13, destabilize the steady state flow with the same structure as the mean flow and induce the Hopf bifurcation.

As can be seen from the disturbance streamlines in Figs. 12 and 13, there are two waves that occupy the periodicity length L and they show a behavior of traveling wave. Then, the wave number is $\alpha = 1.571$ from $L = 8$ and $n = 2$. The frequencies are $\Omega = 0.113$ for $a_u = 2$ and $\Omega = 0.147$ for $a_u = 0$. On the other hand, the frequency of the parallel plates channel ($a_u = a_l = 1$) corresponding to this value of α(in other word, wavelength, $L = 2\pi n/\alpha$) are $\Omega = 0.121$ for $Re = 300$ and $\Omega = 0.139$ for $Re = 130$, respectively. From the relation between the wave number and the frequency, we can consider that the disturbance modes for $a_u = 0$ and 2 are T-S wave modes, although somehow modified due to the need of adaptation to a more complex geometry than parallel plate channel. We can show that the instability mode for $a_u = 0.5$ and 3 are also T-S mode in the same manner.

It is found that the Hopf bifurcation occurs at a quite small Reynolds number for periodically contracted or expanded channel compared with the fact that the plane Poiseuille flow is destabilized by the T-S wave for $Re > 5772$[15, 16]. This is thought to be mainly because a shear layer which is established at the groove lip forces the T-S wave as a result of complex interaction as can be seen in the instantaneous streamlines of self-sustained oscillatory flows.

4.2 Pressure Drop

We consider an effect of contracted or expanded part on the pressure field. The pressure drop Δp and its coefficient λ are defined to study the characteristics of the pressure field as

$$\Delta p = \frac{(p_i^* - p_o^*)}{\rho^* U^{*2}} = p_i - p_o, \tag{10}$$

$$\lambda = \Delta p \frac{h^*}{L^*} = \frac{\Delta p}{L}, \tag{11}$$

where p_i and p_o are the cross-sectional averaged pressure at the inlet and outlet of the periodic module, respectively. The time averaged value is used when the flow field is in time periodic oscillatory state.

For practical applications, it is desirable to compare the pressure drop with corresponding values Δp_p for the parallel plate channel with height $2h^*$. The ratios $\Delta p/\Delta p_p$ of the pressure drops are shown in Fig. 14 for $a_u \geq 1$ and $a_u < 1$, respectively, where the pressure drop for the plane Poiseuille flow is obtained as $\Delta p_p = 2L/Re$ from the velocity profile of $u = 1 - y^2, v = 0$.

As shown in Fig. 14(a), it is emphasized that the pressure drop ratios for $a_u = 1, 2$ and 3 are less than unity for the subcritical Reynolds numbers, thus showing that the effect of the addition of an expanded part to a plane channel is one of drag reduction. This is due to stress relaxation and lack of significant momentum flux at the lip of the expanded part. For the supercritical Reynolds numbers, however, the pressure drop ratio increases above unity as shown in Fig. 14(a). It is seen that the pressure drop ratios show the linear dependency on $(Re - Re_c)$ near the criticality. The Reynolds stress due to flow oscillation is responsible for the increased drag because the Reynolds stress term is quadratic in amplitude of velocity and the amplitude shows the linear dependency as shown in Fig. 6. It is consistent with the previous result of Ghadder et al.[10].

On the other hand, for the case of $a_u = 0$ and 0.5 as shown in Fig. 14(b), the pressure drop ratios are always larger than unity and increase monotonically as the Reynolds number increases. Thus, the addition of the contracted part to the parallel plate channel brings an increase of the pressure drop.

Coefficients of the pressure drop, λ, are depicted in Fig. 15 as a function of the Reynolds number together with some previous results[8, 10]. The coefficient for the plane Poiseuille flow is also shown for reference, where $\lambda = 2/Re$ and is in inverse proportion to the Reynolds number. We can also see in Fig. 15 that for the subcritical Reynolds numbers the coefficients for $a_u \geq 1$ is less than the corresponding quantity for the plane Poiseuille flow, whereas those for $a_u < 1$ is larger than that for the plane Poiseuille flow.

It is also seen in the result of Ghadder et al. for $L = 6.6666, l = 2.2222$, $a_l = 2.1111$ and $a_u = 1$ that the coefficient for the pressure drop are less than the corresponding quantity for the plane Poiseuille flow for the subcritical Reynolds numbers, whereas those for supercritical Reynolds numbers are larger than that for the plane Poiseuille flow, where the critical Reynolds number for the onset of the oscillatory flow is $Re_c = 975$. On the other hand, Wirtz et al.[8] obtained experimentally the coefficients for the parallel plate channel where expanded grooves are symmetrically placed on both the channel walls and each groove is right triangular with depth $2.4h^*$. In this case, the critical Reynolds number for the onset of the oscillatory flow is $Re_c = 177$ and the coefficient for the oscillatory flow regime are shown in Fig. 15. So, they show larger values than our results because the flow becomes better mixed.

5 CONCLUDING REMARKS

A numerical investigation was performed for the flow in channel with periodically contracted or expanded parts as a simple model of plate-type heat exchanger.

The critical Reynolds numbers and frequencies for the onset of self-sustained oscillations are obtained for the various geometric parameters a_u. The analysis of the amplitude dependence of the oscillations on degree of criticality reveals the transition to self-sustained oscillatory flow to be Hopf bifurcation. The frequencies of the oscillatory flow practically agree with that of T-S wave having with the same wave number. The T-S wave modes are thought to be excited by the existence of contracted or expanded parts. In addition, it has been shown that the pressure drop is reduced especially for the channel with the expanded part for the subcritical Reynolds numbers, whereas increased for the supercritical values. On the other hand, it is always increased for the channel with the contracted part.

In this paper, we have confined ourselves to the case of L, l and a_l fixed, where only the effect of a_u is examined for the five different values. Situations are quite different when all the geometric parameters are varied. The critical Reynolds numbers and the pressure drop can be controlled by the geometric factors. The research on such problems is postponed as future works.

Acknowledgment

The authors would like to express our thankful heart to Prof. Y. Ikegami and Ms. N. Visakha for their advises.

References

[1] Kakac, S., Shah R.K. and Aung W. , Handbook of Single-Phase Convective Heat Transfer, A Wiley-Interscience Publication, 1987, Chapter 17.

[2] S. V. Patankar, C. H. Liu and E. M. Sparrow, Fully developed flow and heat transfer in ducts having streamwise-periodic variations of cross-sectional area, ASME J. Heat

Transf.**99**(1977)180-186.

[3] K. M. Kelkar and S. V. Patankar, Numerical prediction of flow and heat transfer in a parallel plate channel with staggered fins, ASME J.Heat Transf.**109**(1987)25-30.

[4] B. Farhanieh and B. Sunden, Numerical investigation of periodic laminar heat transfer and fluid characteristics in parallel plate ducts with streamwise-periodic cavities, Int. J. Num. Meth. Heat Fluid Flow **1**(1991)143-157.

[5] B. Farhanieh, C. Herman and B. Sunden, Numerical and experimental analysis of laminar fluid flow and forced convection heat transfer in a grooved duct, Int. J. Heat Mass Transf. **36**(1993)1609-1617.

[6] E. M. Sparrow and W. Q. Tao, Enhanced heat transfer in a flat rectangular duct with streamwise-periodic disturbances at one principal wall, ASME J. Heat Transf.**105**(1983)851-861.

[7] M. Greiner, R. F. Chen and R. A. Wirtz, Enhanced heat transfer /pressure drop measured from a flat surface in a grooved channel, ASME J.Heat Transf.**113**(1991)498-501.

[8] R. A. Wirtz, F. Huang and M. Greiner, Correlation of fully developed heat transfer and pressure drop in a symmetrically grooved channel, ASME J.Heat Transf.**121**(1999)236-239.

[9] B. Sunden and S. Trollheden, Periodic laminar flow and heat transfer in a corrugated two-dimensional channel, Int. Comm. Heat Mass Transf.**16**(1989)215-225.

[10] N. K. Ghaddar, K. Z. Korczak, B. B. Mikic and A. Y. Patera, Numerical investigation of incompressible flow in grooved channels. Part1. Stability and self-sustained oscillations, J.Fluid Mech.**163**(1986)99-127.

[11] J. C. F. Pereira and J. M. M. Sousa, Finite volume calculations of self-sustained oscillations in a grooved channel, J. Comput. Phys.**106**(1993)19-29.

[12] E. P. L. Roberts, A numerical and experimental study of transition processes in an obstructed channel flow, J. Fluid Mech.**260**(1994)185-209.

[13] J. Mizushima, H. Yamaguchi and H. Okamoto, Stability of flow in a channel with a suddenly expanded part, Phys. Fluids **8**(1996)2933-2942.

[14] P. G. Drazin and W. H. Reid, Hydrodynamic Stability, Cambridge University Press, 1981, Chapter 7.

[15] S. A. Orzsag, Accurate solution of the Orr-Sommerfeld stability equation, J. Fluid Mech.**50**(1971)689-703.

[16] M. Nishioka, S. Iida and Y. Ichikawa, An experimental investigation of the stability of plane Poiseuille flow, J. Fluid Mech.**72**(1975)731-751.

Table 1: Critical Reynolds numbers Re_c and frequencies Ω for various a_u.

a_u	Re_c	Ω_c
3	258	0.115
2	289	0.113
1	409	0.115
0.5	240	0.113
0	123	0.147

Figure captions

Fig.1 Geometries and co-ordinates. (a) Channel with expanded parts in both plates. (b) Channel with expanded parts in one plate. (c) Channel with contracted-expanded parts. (d) Enlargement of part A.

Fig.2 Flow patterns for $a_u = 1$. (a) $Re = 50$. (b) $Re = 380$.

Fig.3 Flow patterns for $a_u = 2$. (a) $Re = 50$. (b) $Re = 260$.

Fig.4 Flow patterns for $a_u = 0$. (a) $Re = 50$. (b) $Re = 100$.

Fig.5 Time evolutions of v for $a_u = 2$. (a) $Re = 250$. (b) $Re = 350$.

Fig.6 Bifurcation diagrams for various a_u

Fig.7 Critical Reynolds numbers for various a_u.

Fig.8 Flow patterns of the self-sustained oscillatory flow during one cycle for $a_u = 2$ and $Re = 300$. (a)$t = t_0 + 0/6T$. (b)$t = t_0 + 1/6T$. (c)$t = t_0 + 2/6T$. (d)$t = t_0 + 3/6T$. (e)$t = t_0 + 4/6T$. (f)$t = t_0 + 5/6T$.

Fig.9 Flow patterns of the self-sustained oscillatory flow during one cycle for $a_u = 0$ and $Re = 130$. (a)$t = t_0 + 0/6T$. (b)$t = t_0 + 1/6T$. (c)$t = t_0 + 2/6T$. (d)$t = t_0 + 3/6T$. (e)$t = t_0 + 4/6T$. (f)$t = t_0 + 5/6T$.

Fig.10 Time averaged flow patterns of one cycle for $a_u = 2$ and $Re = 300$.

Fig.11 Time averaged flow patterns of one cycle for $a_u = 0$ and $Re = 130$.

Fig.12 Contours of disturbance for $a_u = 2$ and $Re = 300$. (a)$t = t_0 + 0/6T$. (b)$t = t_0 + 1/6T$. (c)$t = t_0 + 2/6T$. (d)$t = t_0 + 3/6T$. (e)$t = t_0 + 4/6T$. (f)$t = t_0 + 5/6T$.

Fig.13 Contours of disturbance for $a_u = 0$ and $Re = 130$. (a)$t = t_0 + 0/6T$. (b)$t = t_0 + 1/6T$. (c)$t = t_0 + 2/6T$. (d)$t = t_0 + 3/6T$. (e)$t = t_0 + 4/6T$. (f)$t = t_0 + 5/6T$.

Fig.14 The pressure drop ratio. (a) $a_u \geq 1$. (b) $a_u < 1$.

Fig.15 Coefficients of the pressure drop.

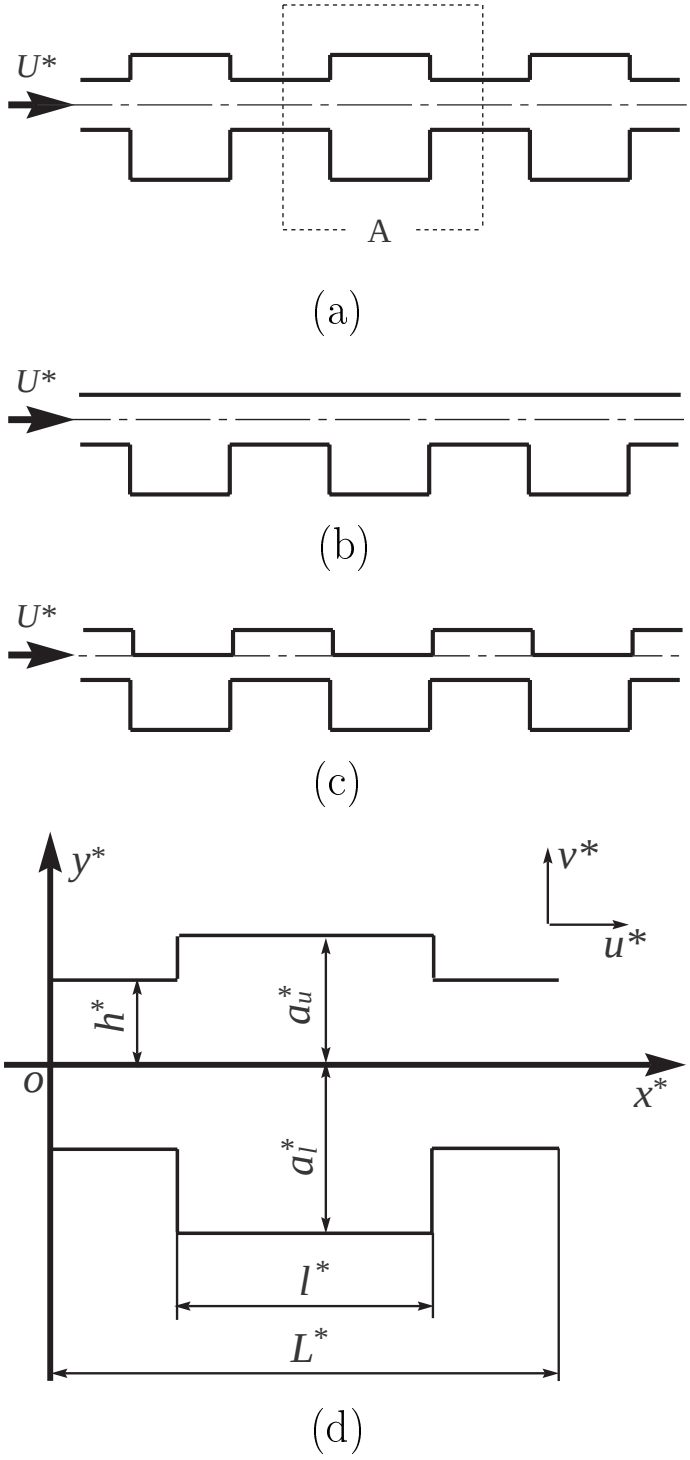

Figure 1: T. Adachi and H. Uehara

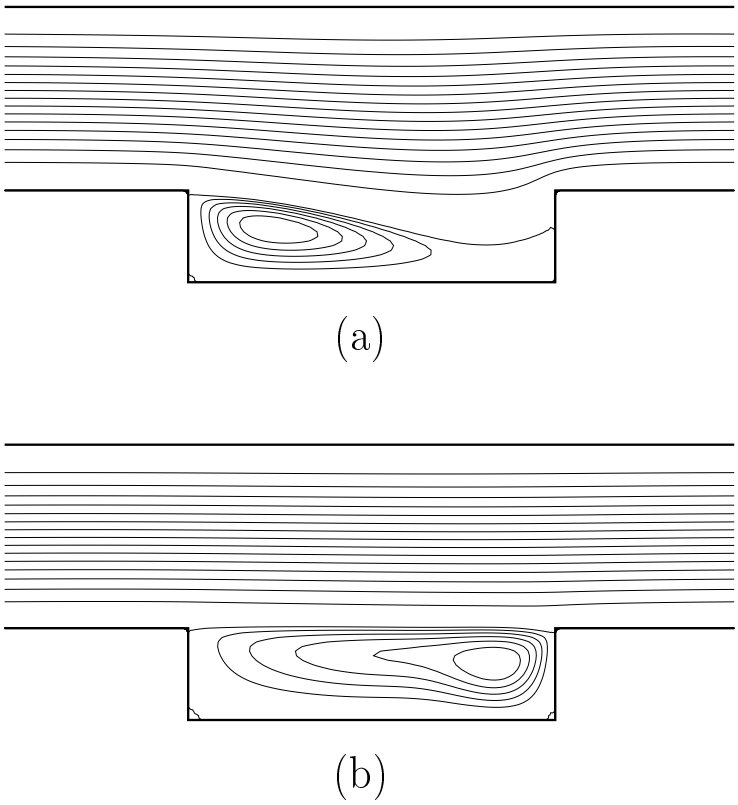

Figure 2: T. Adachi and H. Uehara

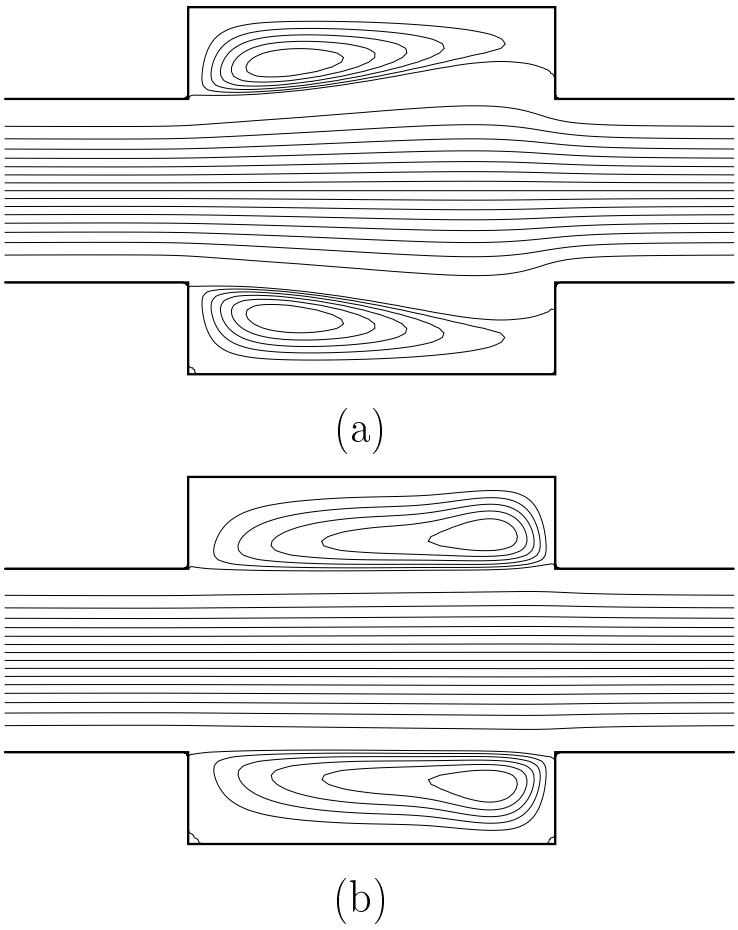

Figure 3: T. Adachi and H. Uehara

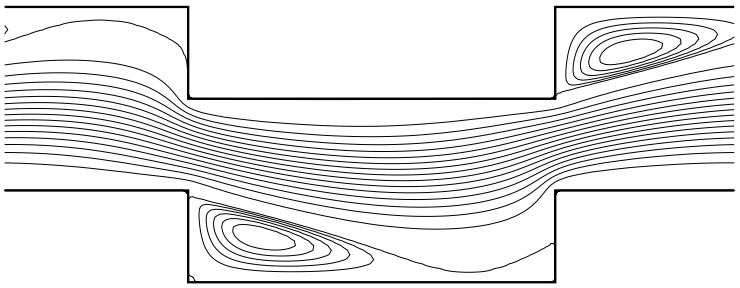

(a)

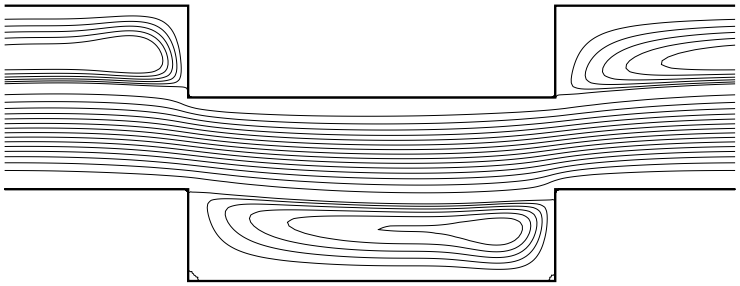

(b)

Figure 4: T. Adachi and H. Uehara

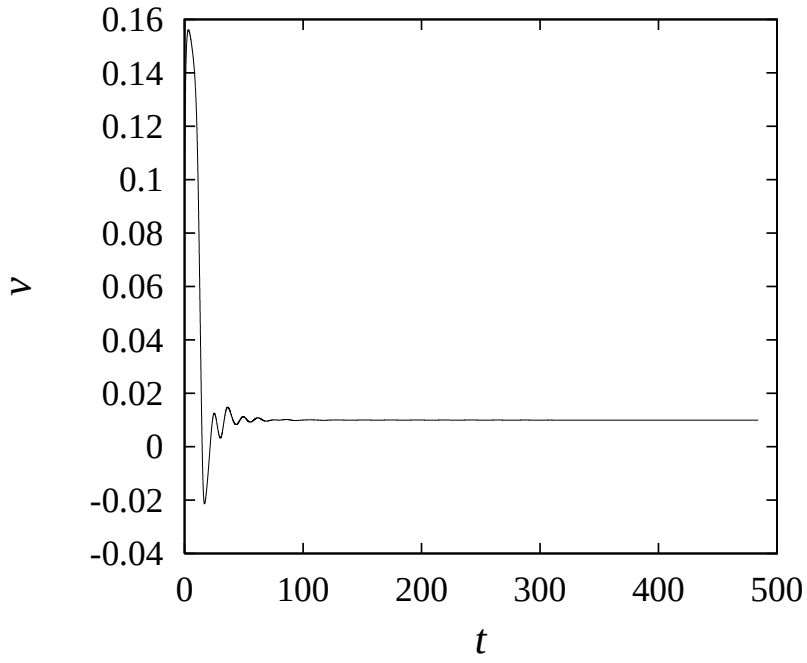

(a)

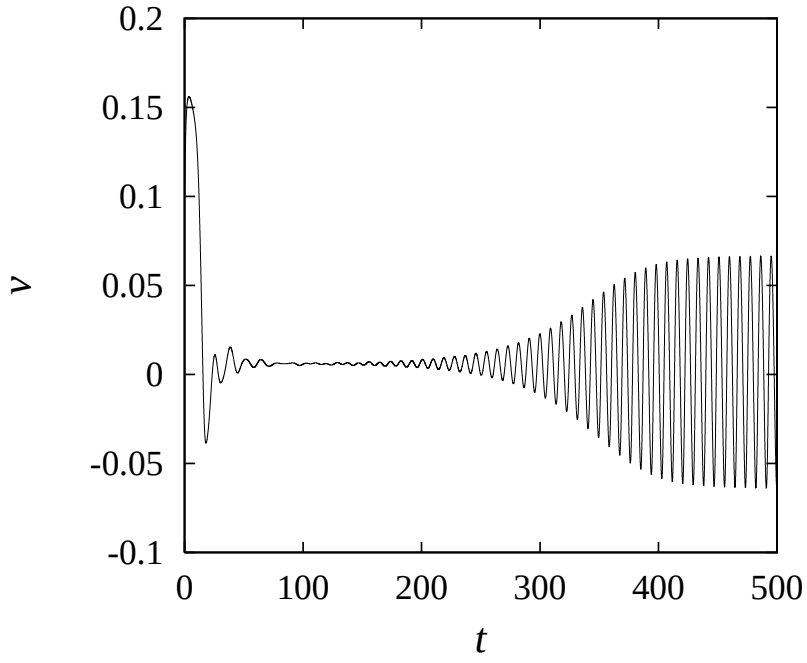

(b)

Figure 5: T. Adachi and H. Uehara

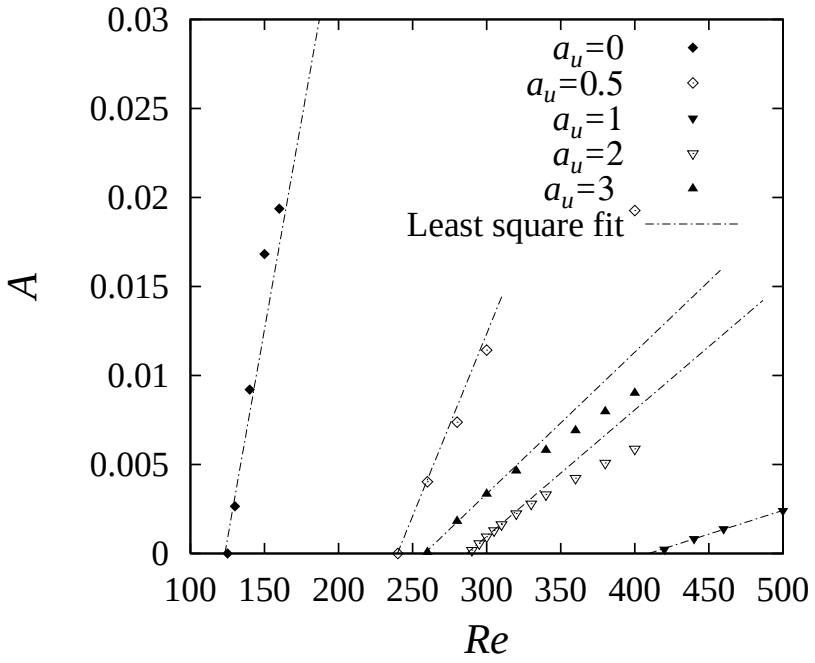

Figure 6: T. Adachi and H. Uehara

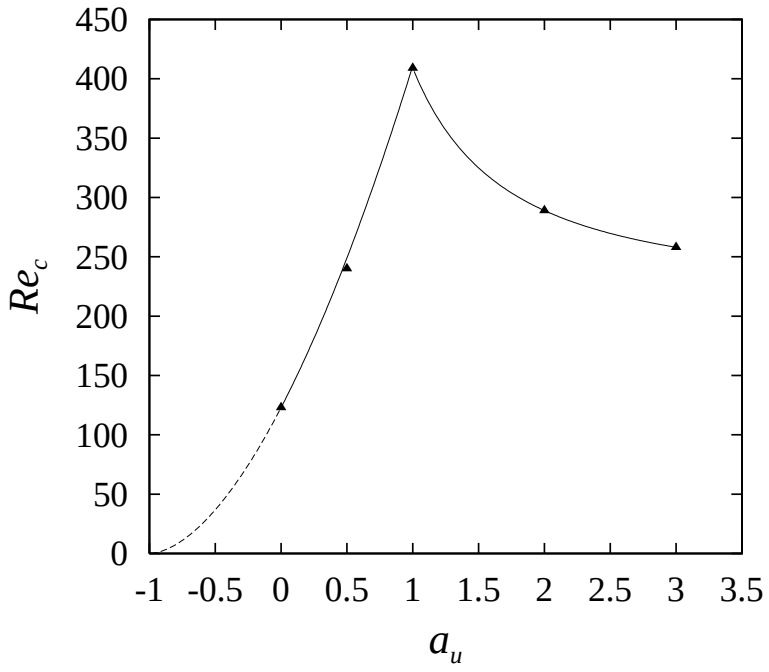

Figure 7: T. Adachi and H. Uehara

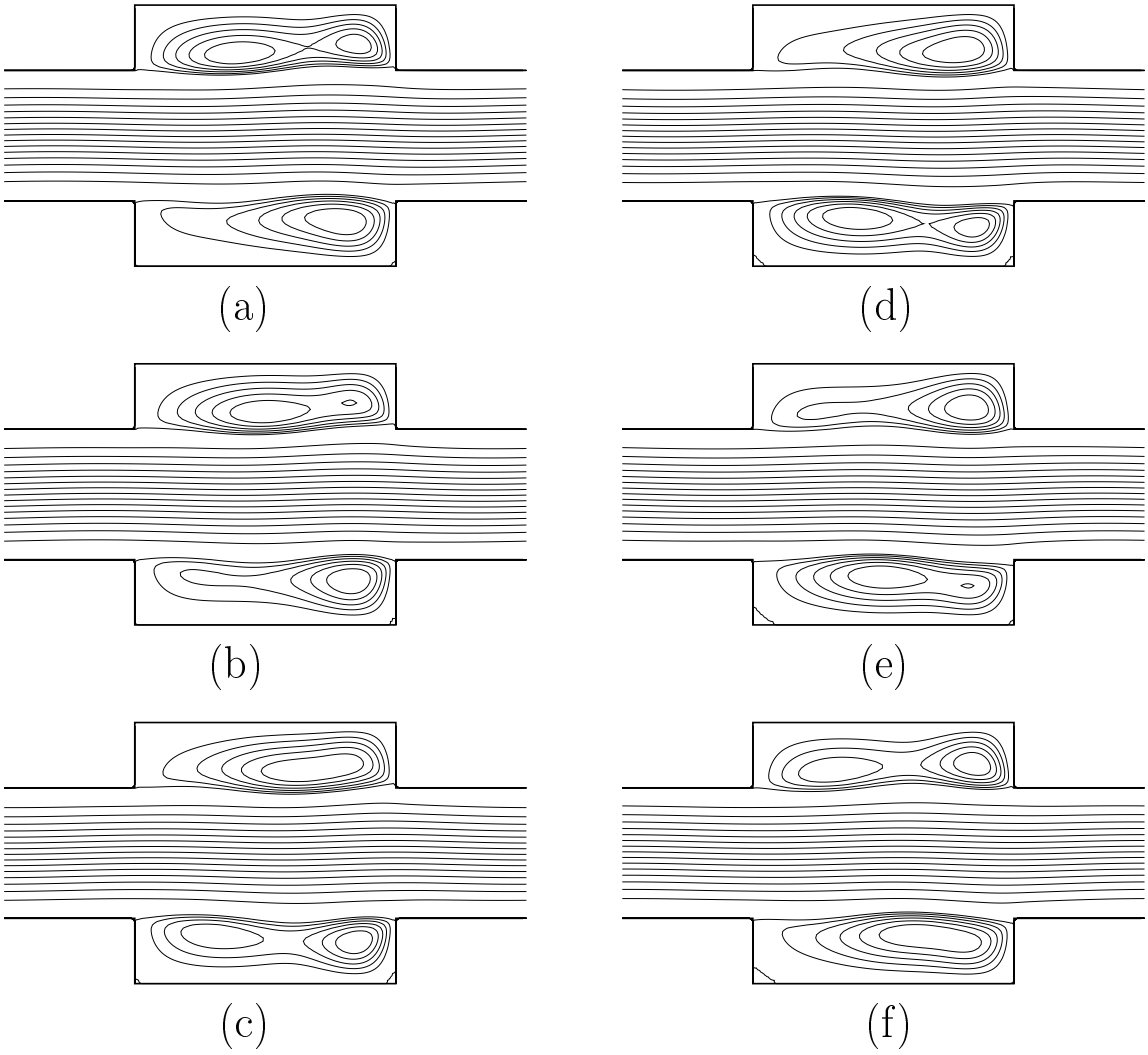

Figure 8: T. Adachi and H. Uehara

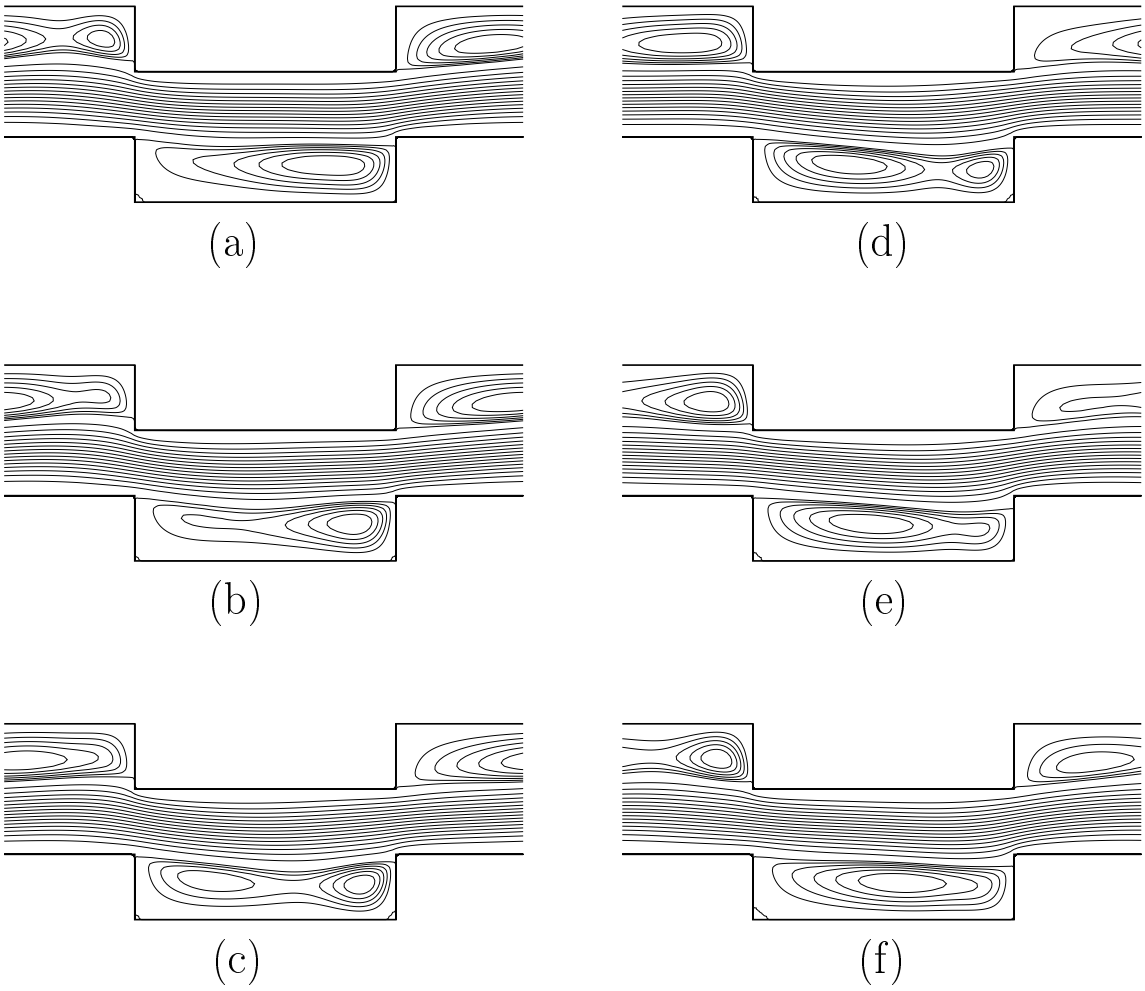

Figure 9: T. Adachi and H. Uehara

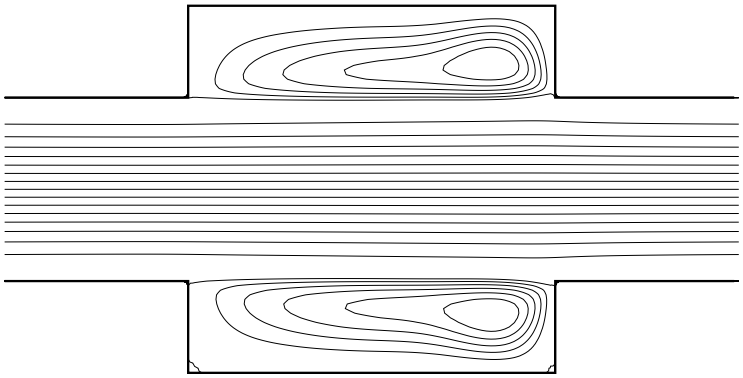

Figure 10: T. Adachi and H. Uehara

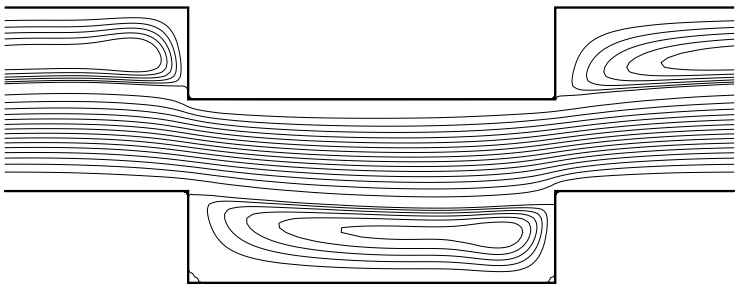

Figure 11: T. Adachi and H. Uehara

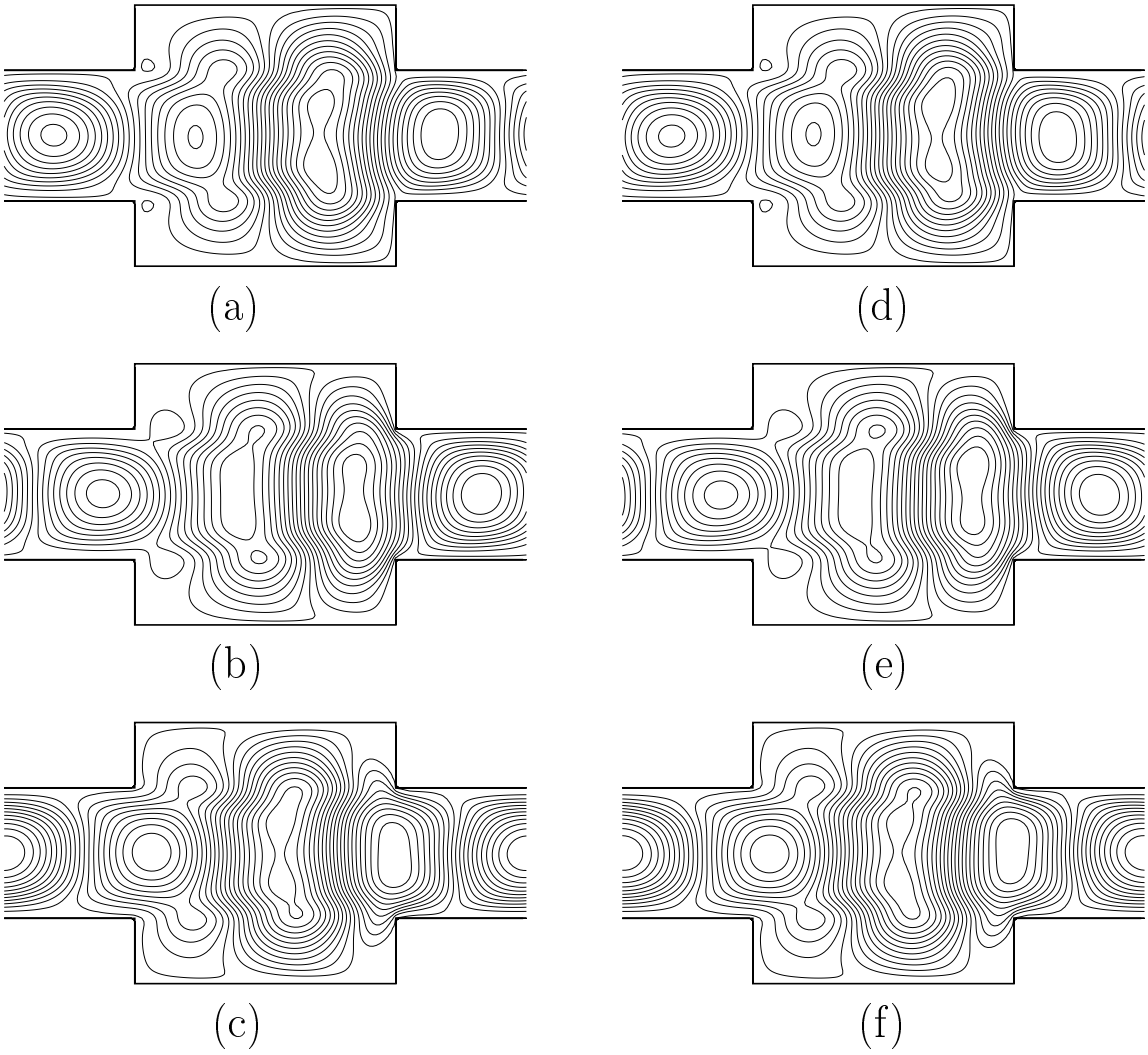

Figure 12: T. Adachi and H. Uehara

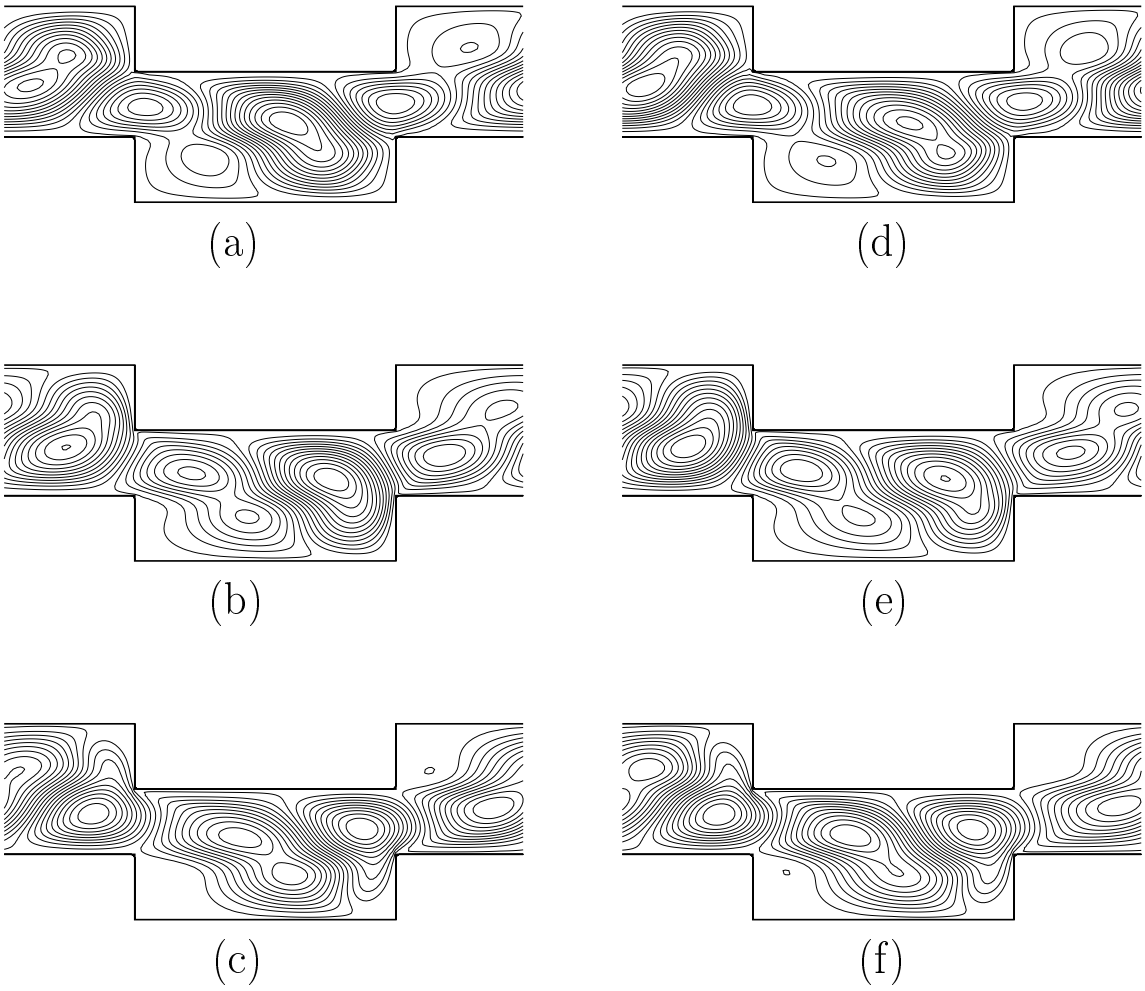

Figure 13: T. Adachi and H. Uehara

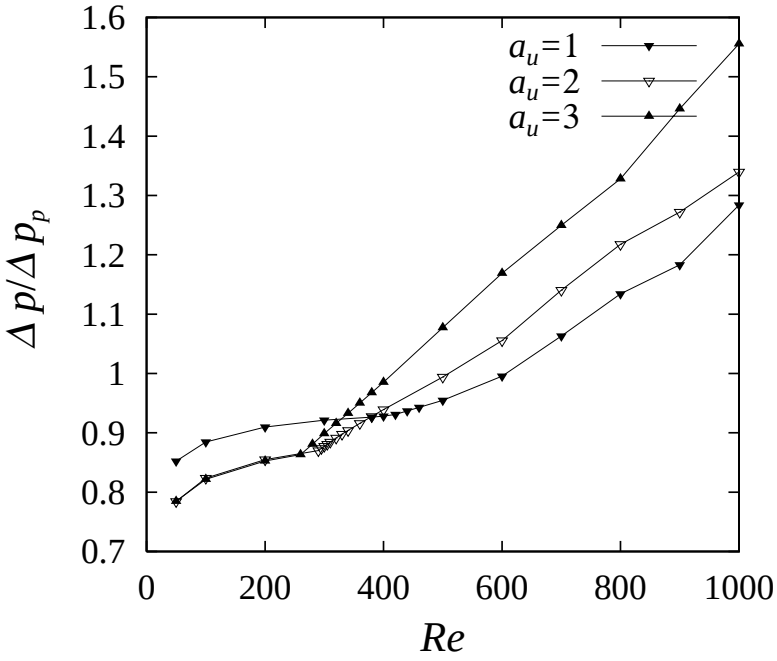

(a)

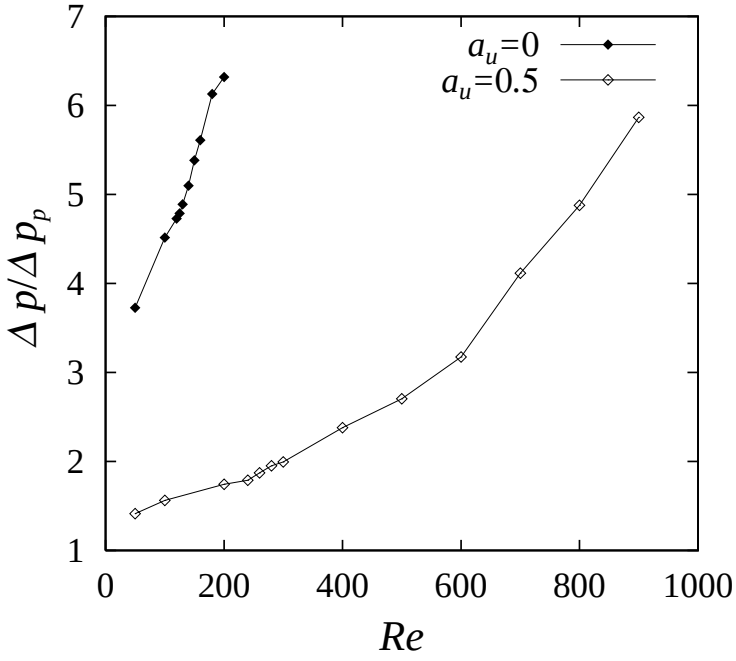

(b)

Figure 14: T. Adachi and H. Uehara

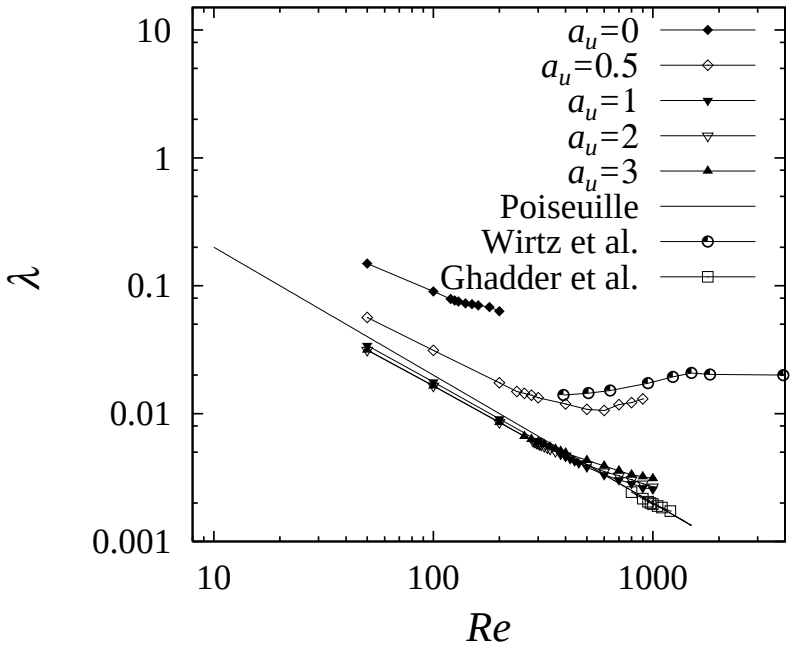

Figure 15: T. Adachi and H. Uehara